Vortex stability in interacting Bose-Einstein condensates

Ajay Srinivasan,* Aaron Wirthwein,† and Stephan Haas‡
Department of Physics and Astronomy, University of Southern California, Los Angeles, CA 90007

(Dated: September 12, 2024)

Abstract: We study the formation and stability of vortices in a binary system of Bose-Einstein condensates, with their wavefunctions modeled by a set of coupled, time-dependent Gross-Pitaevskii equations. Beginning with an effective two-dimensional system, we identify miscible and immiscible regimes characterized by the inter- and intra-atomic interactions and the initial configuration of the system. We then consider a binary system of Bose-Einstein condensates placed in a rotating harmonic trap and study the single vortex state in this system. We derive an approximate form for the energy of a single vortex in the binary system and the critical angular velocity for the global stability of a vortex at the center of the trap. We also compute the metastability onset angular velocity for the local stability of a vortex at the center of the trap. Numerical solutions to the Gross-Pitaevskii equations support these expressions. These rotational results inform us of a novel subphase within the miscible regime of the binary condensate system. We thus demonstrate the non-trivial aspects of vortex stability in interacting binary Bose-Einstein condensates as a result of their non-linear interactions.

I. INTRODUCTION

The study of Bose-Einstein condensates (BECs) has significantly advanced our understanding of quantum mechanics on a macroscopic scale, revealing complex behaviors that are both theoretically interesting and experimentally observable. Among these behaviors, the formation and dynamics of vortices are particularly notable due to their complexity and relevance to quantum fluid dynamics. In previous work on the collision dynamics of one-dimensional Bose-Einstein condensates, we analyzed the interactions of two colliding BECs using coupled, time-dependent Gross-Pitaevskii equations [1]. This investigation demonstrated how the interplay between inter- and intra-atomic interactions and initial configurations led to different dynamical regimes, from periodic transmission or reflection of condensates to more complex transient dynamics.

In this paper, we extend our study to a two-dimensional system to explore vortex formation and stability within a binary system of interacting Bose-Einstein condensates. We first restrict ourselves to a binary system of vortex-free condensates – modeling their wavefunctions with coupled, time-dependent Gross-Pitaevskii equations and identify phases based on atomic interactions and initial system configurations. Next, we examine a binary BEC system in a rotating harmonic trap, using a step-by-step analysis, focusing on single vortex formation and stability. We derive an approximate form for the energy a single vortex in a trapped system and determine the critical angular velocities for the global and local stability of a vortex at the trap center, supported by numerical solutions to the Gross-Pitaevskii equations. This study demonstrates the complex behavior of vortex dynamics in binary Bose-Einstein condensates due to their non-linear interactions, which should be observable under appropriate laboratory conditions.

Our investigation builds on several previous studies, addressing rotating trapped Bose-Einstein condensates [2–4]. These earlier works showed how rotating traps introduce discrete quantized vorticity, leading to vortex arrays and complex condensate behaviors under varying rotational speeds. They also developed efficient numerical methods for simulating these dynamics, emphasizing the conservation of angular momentum and the stability of vortex states. Our current study extends these insights by examining vortex formation and stability in interacting binary BEC systems, providing a deeper understanding of these quantum systems and their potential applications.

The paper is organized as follows. In section II, we first discuss the formation of miscible and immiscible steady states in the absence of vortices. In section III, we analyze the formation and stability of vortices in rotating condensates, including the effect of a trapping potential. The theoretical analysis in subsections III A, III B, and III C is complemented by numerical simulations in subsection III D, and it indicates a critical angular velocity which separates regimes of stable, metastable, and unstable vortices. In subsection III E, we present a discussion of the results from our approach, particularly noting a novel phenomenon we term the *dumbbell phase* within the miscible regime, informed by vortex stability. In IV, we summarize our results, discuss limitations of our approach, and possible extensions of the framework to study broader classes of vortices and vortex lattices as in [2–8].

* avsriniv@usc.edu
† wirthwei@usc.edu
‡ shaas@usc.edu

II. TWO INTERACTING VORTEX-FREE CONDENSATES

Let us start by considering the formation of miscible and immiscible states in two interacting condensates composed of N ^{87}Rb atoms in the hyperfine spin states $|1\rangle = |1,-1\rangle$ and $|2\rangle = |2,1\rangle$ [1]. We then write a_{11} for the s-wave scattering length of a condensate composed of atoms in the $|1\rangle$ state, and a_{22} for the s-wave scattering length of a condensate with atoms in the $|2\rangle$ state. The inter-atomic interaction between the condensates is parametrized by a scattering length a_{12} (see Table I in [9] for experimentally measured values of a_{12}). We consider a harmonic potential trap,

$$V(\mathbf{r}) = \frac{1}{2}m(\omega_x^2 x^2 + \omega_y^2 y^2 + \omega_z^2 z^2), \tag{1}$$

where m is the mass of Rubidium. The trap is designed with the z-confinement sufficiently large, so that the system is effectively two-dimensional in the $x-y$ plane. That is, ω_z is large enough so that the condensate is forced into the ground state along the z direction but is free to explore excited states in the x and y directions. Furthermore, we initially focus on systems with vortex-free ground states. In section III, we derive criteria which the trap must satisfy to ensure that this is the case, but for now one may think of this as the study of a non-rotating trap or a sufficiently slow-spinning trap.

Plotting Parameters	
Quantity	Value or Expression
a_{11}	$100.4a_0$
a_{22}	$98.006a_0$
m	87 amu
$\omega_\perp$	$2\pi \times 10$
Atom number	1000

TABLE I: A table of parameters used to plot quantities throughout this work (particularly in Figs. 4 and 5). Here a_{jj} is the intra-atomic scattering length of the j-th condensate, m is the mass of a ^{87}Rb atom, $\omega_\perp$ is the trap frequency, and a_0 is the Bohr radius.

The effectively two-dimensional dynamics of two vortex-free Rubidium condensates occupying different hyperfine spin states is modeled using the coupled Gross-Pitaevskii equations [1] [10],

$$i\hbar\frac{\partial\psi_1}{\partial t} = \left(-\frac{\hbar^2}{2m}\nabla^2 + V + Ng_{11}|\psi_1|^2 + Ng_{12}|\psi_2|^2\right)\psi_1, \tag{2}$$

$$i\hbar\frac{\partial\psi_2}{\partial t} = \left(-\frac{\hbar^2}{2m}\nabla^2 + V + Ng_{22}|\psi_2|^2 + Ng_{12}|\psi_1|^2\right)\psi_2, \tag{3}$$

where N is the atom number, ψ_1 and ψ_2 are the 2D wave functions describing the $|1\rangle$ and $|2\rangle$ condensates respectively, and g_{ij} are the re-normalized interaction parameters introduced in [1].

We seek to understand how g_{12}, ω_x, and ω_y affect the dynamics of the system late in the time-evolution, as a steady state is approached. Let us first identify the quasi-static phases of the system, using methods similar to those in [1]. We begin with the energy functional,

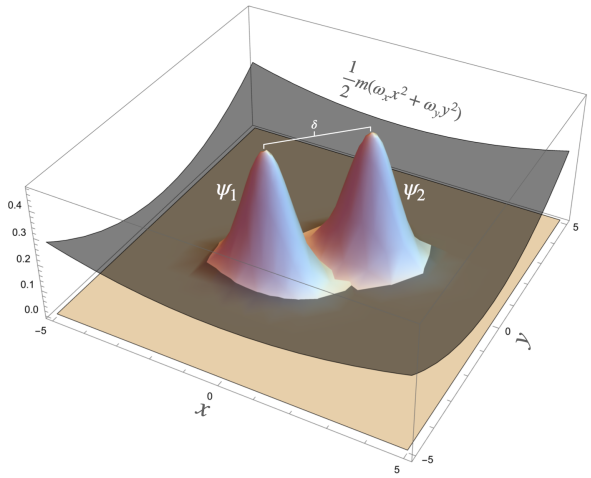

FIG. 1: Initial configuration of two condensates with Gaussian profiles, denoted by ψ_1 and ψ_2, in a harmonic potential trap $V(x,y) = \frac{1}{2}m(\omega_x x^2 + \omega_y y^2)$. Here, δ is the distance between the centers of the condensates.

$$E = \iint \mathrm{d}A \left(\sum_{i=1,2} \left(\frac{\hbar^2}{2m}|\nabla\psi_i|^2 + V|\psi_i|^2 + \frac{g_{ii}|\psi_j|^4}{2} \right) + g_{12}|\psi_1|^2|\psi_2|^2 \right). \tag{4}$$

We now apply the variational method to investigate ground state properties of this system [1], considering the Gaussian ansatz,

$$\psi_j = \frac{1}{\sqrt{\pi\sigma_{jx}\sigma_{jy}}} \exp\left(-\frac{(x-x_j)^2}{2\sigma_{jx}^2}\right) \exp\left(-\frac{(y-y_j)^2}{2\sigma_{jy}^2}\right). \tag{5}$$

Here, for each $j = 1, 2$, σ_{jx} and σ_{jy} are variational parameters describing the width of the Gaussian in the x and the y directions respectively, while x_j and y_j are variational parameters describing the central location of the Gaussian.

Inserting (5) into (4), we find:

$$\begin{aligned} E = &\frac{N\hbar^2}{4m}\left(\frac{1}{\sigma_{1x}^2}+\frac{1}{\sigma_{1y}^2}+\frac{1}{\sigma_{2x}^2}+\frac{1}{\sigma_{2y}^2}\right) \\ &+\frac{N}{4}m\omega_x^2(\sigma_{1x}^2+2x_1^2+\sigma_{2x}^2+2x_2^2) \\ &+\frac{N}{4}m\omega_y^2(\sigma_{1y}^2+2y_1^2+\sigma_{2y}^2+2y_2^2) \\ &+\frac{N^2}{4\pi}\left(\frac{g_{11}}{\sigma_{1x}\sigma_{1y}}+\frac{g_{22}}{\sigma_{2x}\sigma_{2y}}\right) \\ &+\frac{N^2 g_{12}\exp\left(-\left(\frac{\delta_x^2}{(\sigma_{1x}^2+\sigma_{2x}^2)}+\frac{\delta_y^2}{(\sigma_{1y}^2+\sigma_{2y}^2)}\right)\right)}{\pi\sqrt{(\sigma_{1x}^2+\sigma_{2x}^2)(\sigma_{1y}^2+\sigma_{2y}^2)}}. \end{aligned} \tag{6}$$

Here we have defined $\delta_x \equiv x_1 - x_2$ and $\delta_y \equiv y_1 - y_2$. The ground state conditions for the system can now be obtained using a variational analysisA, beginning from (6). For the remainder of this section, we assume that $g_{11} = g_{22} \equiv g$. Suppose at least one of δ_x and δ_y is non-zero (without loss of generality, let $\delta_x \neq 0$). Under this assumption, we find that $\sigma_{1x} = \sigma_{2x} = \sigma_x$ and $\sigma_{1y} = \sigma_{2y} = \sigma_y$. We then obtain a balance relation between the widths of the condensates in the x and y directions,

$$\sigma_x\omega_x = \sigma_y\omega_y. \tag{7}$$

This analysis is restricted to the case of separation solely in the x-direction, i.e.,$\delta_y = 0$, and $\delta := \delta \geq 0$. In appendix A, we obtain Taylor approximations for σ_x, σ_y, and δ in the large N limit, where the kinetic energy contributions to the ground state conditions may be neglected. These approximations lead to

$$\sigma_x^4 = \frac{N\omega_y}{m\pi\omega_x^3}\frac{g+g_{12}}{2}, \tag{8}$$

$$\sigma_y^4 = \frac{N\omega_x}{m\pi\omega_y^3}\frac{g+g_{12}}{2}, \tag{9}$$

$$\delta = \left(\frac{2N\omega_y}{m\pi\omega_x^3}(g+g_{12})\right)^{1/4}\sqrt{\log_e\left(\frac{g_{12}}{g}\right)}. \tag{10}$$

Eq. (10) indicates a phase transition at $g_{12} = g$. For $g_{12} < g$, we see that $\delta_x = \delta_y = 0$ must necessarily be true. For $g_{12} > g$, the ground state solutions are approximately described by the above analysis.

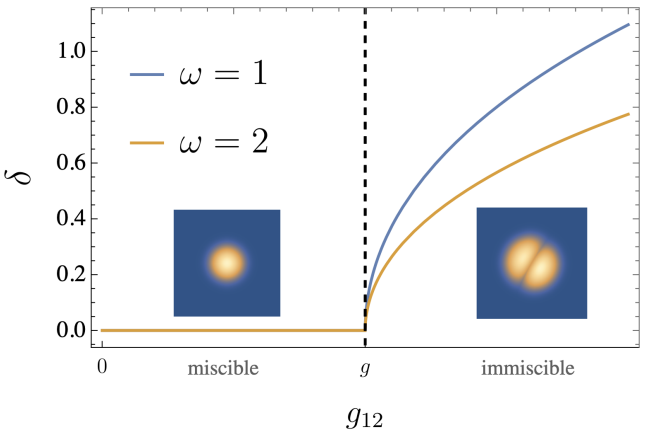

FIG. 2: Dependence of the distance between the condensate centers, δ, on the inter-condensate repulsion strength g_{12} and on the trap frequency ω (within the approximations considered in section II). Here, we consider the case where the trap frequency within the $x-y$ plane is $\omega = \omega_x = \omega_y$, and we set $2N/m\pi = 1$ and $g = 1$. The dotted vertical line demarcates the critical point at $g_{12} = g$. For $g_{12} < g$, the system is in a miscible phase shown by the inset on the left. For $g_{12} > g$, the system is in an immiscible regime illustrated by the inset on the right.

III. TWO INTERACTING ROTATING CONDENSATES

A. Theoretical Model in Uniform Medium

Next we address the vortex dynamics of binary condensate systems in a harmonic trap, again considering two condensates composed of N ^{87}Rb atoms in the hyperfine spin states $|1\rangle = |1,-1\rangle$ and $|2\rangle = |2,1\rangle$. Let g_{11}, g_{22}, and g_{12} be the interaction parameters, as used in section II. We first focus on the single vortex dynamics in a free system ($V \equiv 0$) with $g_{12} < \sqrt{g_{11}g_{22}}$, i.e., the condensates are in the mixing regime.

To proceed with the analysis of the GPEs, we switch to cylindrical coordinates, letting $\psi_j = f_j(\rho)e^{il\varphi}$, so that $|\psi_j| = f_j(\rho)$. Here l is a non-negative integer describing the quantum of circulation of the vortex in question. The time-independent GPEs [11] for the system are

$$-\frac{\hbar^2}{2m\rho}\frac{\mathrm{d}}{\mathrm{d}\rho}\left(\rho\frac{\mathrm{d}f_1}{\mathrm{d}\rho}\right)+\frac{\hbar^2 l^2 f_1}{2m\rho^2}+g_{11}f_1^3+g_{12}f_2^2f_1 = \mu_1 f_1, \tag{11}$$

$$-\frac{\hbar^2}{2m\rho}\frac{\mathrm{d}}{\mathrm{d}\rho}\left(\rho\frac{\mathrm{d}f_2}{\mathrm{d}\rho}\right)+\frac{\hbar^2 l^2 f_2}{2m\rho^2}+g_{22}f_2^3+g_{12}f_1^2f_2 = \mu_2 f_2. \tag{12}$$

Here μ_j are the chemical potentials of each condensate. We now focus on vortices with $l = 1$. At sufficiently large radial distances, the $1/\rho^2$ terms and radial derivatives may be neglected. Therefore, for large ρ the GPEs reduce to a pair of coupled linear equations, which can be solved to yield asymptotic (in ρ) solutions,

$$f_1 \sim \frac{g_{22}\mu_1 - g_{12}\mu_2}{g_{11}g_{22}-g_{12}^2}, \tag{13}$$

$$f_2 \sim \frac{g_{11}\mu_2 - g_{12}\mu_1}{g_{11}g_{22}-g_{12}^2}. \tag{14}$$

We now define the right hand side of (13) to be n_1 and the right hand side of (14) to be n_2, so that n_j is the j-th condensate's density far from the vortex. We then rescale the system based on the healing lengths of the condensates, and the 'far-off' densities n_j. We define the aggregate healing length $\xi \equiv \sqrt{\xi_1 \xi_2}$, where ξ_j is the healing length of the j-th condensate. Thus we identify a new scaled distance parameter $x \equiv \rho/\xi$ and scaled wave function amplitudes $\chi_j = f_j/\sqrt{n_j}$.

We now aim to perform a variational approach on the energy functional,

$$E = \iint \mathrm{d}A \left\{ \sum_{j=1,2} \left(\frac{\hbar^2}{2m} \left(\frac{\mathrm{d}f_j}{\mathrm{d}\rho} \right)^2 + \frac{\hbar^2}{2m} \frac{f_j^2}{\rho^2} \right) + \frac{g_{11}}{2} f_1^4 + \frac{g_{22}}{2} f_2^4 + g_{12} f_1^2 f_2^2 \right\}. \tag{15}$$

Using the rescaled objects defined above, we find that the vortex energy per unit length can be written as

$$\begin{aligned} \epsilon_v = \frac{\pi\hbar^2}{m} \int_0^{\frac{D}{\xi}} x\mathrm{d}x \Bigg[& n_1 \sqrt{n_1 g_{11} n_2 g_{22}} \left(\frac{d\chi_1}{dx} \right)^2 \\ & + n_1 \sqrt{n_1 g_{11} n_2 g_{22}} \frac{\chi_1^2}{x^2} + n_2 \sqrt{n_1 g_{11} n_2 g_{22}} \left(\frac{d\chi_2}{dx} \right)^2 \\ & + n_2 \sqrt{n_1 g_{11} n_2 g_{22}} \frac{\chi_2^2}{x^2} + \frac{n_1^2 g_{11}}{2} (1-\chi_1^2)^2 \\ & + \frac{n_2^2 g_{22}}{2} (1-\chi_2^2)^2 + n_1 n_2 g_{12} (1-\chi_1^2)(1-\chi_2^2) \Bigg], \end{aligned} \tag{16}$$

where D is a large cutoff distance. Applying the trial functions $\chi_j = x/(\alpha_j + x^2)^{1/2}$, which obey $\chi_j \to 1$ as $x \to \infty$, we obtain a minimum at about $\alpha_j = 2$. For this point, we get

$$\begin{aligned} \epsilon_v = & \frac{\pi\hbar^2}{m} n_1 \left(\frac{1}{2} \sqrt{\frac{n_1 g_{11}}{n_2 g_{22}}} + \log_e \left(\beta \frac{D}{\xi} \right) \right) \\ & + \frac{\pi\hbar^2}{m} n_2 \left(\frac{1}{2} \sqrt{\frac{n_2 g_{22}}{n_1 g_{11}}} + \log_e \left(\beta \frac{D}{\xi} \right) \right) \\ & + \frac{\pi\hbar^2}{m} g_{12} \sqrt{\frac{n_1 n_2}{g_{11} g_{22}}}, \end{aligned} \tag{17}$$

where $\beta = 0.908$ is a numerical constant. Refer to Fig. 6 for a plot of this ansatz, along with a numerical solution of the differential equations that will be discussed below.

As a quick check, let us consider the limit $g_{12} = 0$, $n_1 = n_2 = n$, and $g_{11} = g_{22}$, i.e., a system of two identical non-interacting free condensates. In this case, $\epsilon_v = \frac{2\pi\hbar^2 n}{m} \log_e \left(1.497 \frac{D}{\xi} \right)$, twice the variational result seen in [11], as expected. This limit also gives us a way to sharpen the numerical constant β in (17). Ref. [11] determines the GPEs for a single free condensate with a vortex, similar to Eqs. (11) (12), computationally to obtain the vortex energy per unit length of $\pi n \frac{\hbar^2}{m} \log_e \left(1.464 \frac{D}{\xi} \right)$. We can now propose thus a sharper value for β in Eq. (17) to be 0.888. The expression obtained with this value matches the computational result of Ref. [11] in the required limit. From here on, we therefore use Eq. (17) with $\beta = 0.888$ for the vortex energy per unit length.

B. Theoretical Model in a Harmonic Trap

We now extend our analysis the system in the previous section, by considering an additional external potential trap of the form $V = \frac{1}{2} m \omega_\perp \rho^2$ where $\omega_\perp$ is the trap frequency, and we carry out an analysis along the lines of the one conducted in Ref. [11]. Here we assume that the number of atoms in each condensate is large enough so that the Thomas-Fermi approximation is an adequate description of the system. Under these circumstances, in appendix B 1 we show that the size of the vortex core, determined by the healing lengths, is much smaller than the radius of each condensate. This is done using the relations

$$\frac{\hbar^2}{2m\xi_{0,j}^2} = n_j(0) g_{jj}, \tag{18}$$

$$\mu_j = \frac{1}{2} m \omega_\perp R_j^2, \tag{19}$$

where $\xi_{0,j}$ is the healing length of the j-th condensate at the center, $n_j(0)$ is the density of the j-th condensate at the center in the absence of rotation, μ_j is the chemical potential of the j-th condensate, and R_j is the radius of the j-th condensate. In the absence of ambiguity, we refer to $\xi_{0,j}$ by ξ_j and to $n_j(0)$ by n_j.

Up to an intermediate distance ρ_0, the vortex energy can be approximated quite well by the results in appendix III A ((17) particularly), provided ρ_0 is much larger than the vortex core size and much smaller than the radius of the condensates, i.e., $\sqrt{\xi_1 \xi_2} \ll \rho_0 \ll \min\{R_1, R_2\}$. At larger distances, while the condensate densities are unaffected by the vortex, the condensates move at speeds determined by the quantized circulation about the vortex. This extra energy can be approximated using a hydrodynamic kinetic term,

$$\begin{aligned} \epsilon_v = \epsilon_u(\rho_0) + \frac{1}{2} m \Bigg(& \int_{\rho_0}^{R_1} n_1(r) v^2(r) 2\pi r \, \mathrm{d}r \\ & + \int_{\rho_0}^{R_2} n_2(r) v^2(r) 2\pi r \, \mathrm{d}r \Bigg), \end{aligned} \tag{20}$$

where $\epsilon_u(\rho_0)$ is the vortex energy in a uniform medium (as in Eq. (17)) evaluated at cutoff distance ρ_0, $v(r) =$

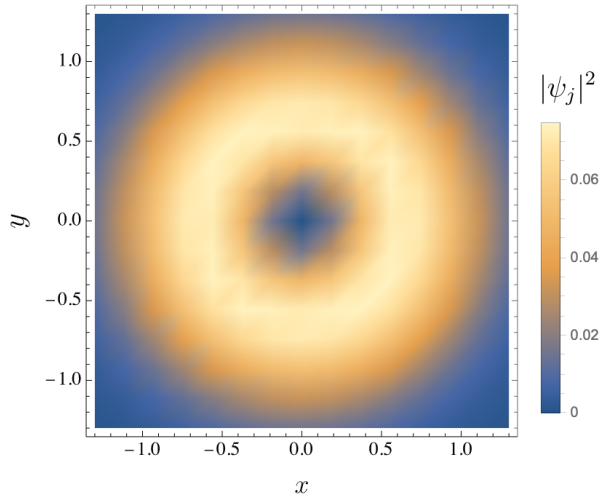

FIG. 3: Density plot of the profile of two mixing condensates with a single quantized vortex in a harmonic trap $V = \frac{1}{2}m\omega_\perp(\rho^2)$, where $\rho^2 = x^2 + y^2$, as considered in III B. Here we take the radii of both condensates to be equal. Up to an intermediate distance $\sqrt{\xi_1\xi_2} \ll \rho_0 \ll R$, where R is the common radius, and ξ_j are the healing lengths of the j-th condensate, the radial profile of the system is well approximated by $r/(2+r^2)^{1/2}$, where $r = \rho/\sqrt{\xi_1\xi_2}$. Beyond ρ_0, the profile of the system is dictated by hydrodynamic effects from the vortex circulation, i.e. it decays to 0 as we approach R.

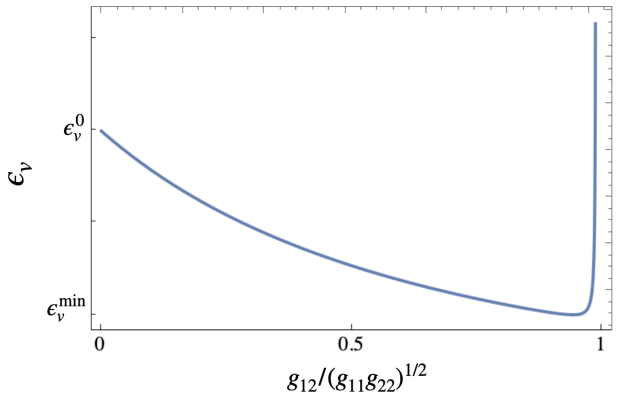

FIG. 4: Vortex energy (per unit length) ϵ_v for a system of two mixing condensates with a singly quantized on-center vortex in a harmonic trap as a function of the scaled interaction parameter $g_{12}/\sqrt{g_{11}g_{22}}$. The value 0 on the horizontal axis corresponds to the absence of inter-condensate interaction, i.e., the single condensate limit, whereas the value 1 corresponds to the transition point to the immiscible regime. On the vertical axis, $\epsilon_v^{\min}$ corresponds to the minimal vortex energy of the system, attained just before the transition point. ϵ_v^0 corresponds to the vortex energy in the absence of inter-condensate interaction.

$\frac{\hbar}{mr}$ is the hydrodynamic speed, and $n_j(r) = n_j \cdot \left(1 - \frac{(g_{ii}-g_{12})r^2}{g_{ii}R_j^2 - g_{12}R_i^2}\right)$ (again we use the convention $i \neq j$, and $i, j \in \{1, 2\}$).

Evaluating these integrals and adding them to the uniform medium result in the simplifying equal radius case, $R_1 = R_2 =: R$, we find

$$\begin{aligned}\epsilon_v = &\frac{\pi\hbar^2}{m}n_1\left(\frac{1}{2}\sqrt{\frac{n_1 g_{11}}{n_2 g_{22}}} + \log\left(0.539\frac{R}{\xi}\right)\right)\\ &+ \frac{\pi\hbar^2}{m}n_2\left(\frac{1}{2}\sqrt{\frac{n_2 g_{22}}{n_1 g_{11}}} + \log\left(0.539\frac{R}{\xi}\right)\right)\\ &+ \frac{\pi\hbar^2}{m}g_{12}\sqrt{\frac{n_1 n_2}{g_{11}g_{22}}}.\end{aligned} \tag{21}$$

The integrals in Eq.(20) can also be evaluated fairly easily when $R_1 \neq R_2$, and the results are presented in appendix B 2 - these details have been omitted from this section for ease of presentation.

We now make a brief note regarding off-axis vortices, located at a radius b from the center in the equal radius setup. In this case, the condensate densities scale like $\left(1 - \frac{b^2}{R^2}\right)$, and we find that $\epsilon_v(b) = \left(1 - \frac{b^2}{R^2}\right)\epsilon_v$, where ϵ_v is the result in Eq.(21). We also compute the total angular momentum of the system, which is given by

$$\mathcal{L} = \hbar\left(\int_0^{R_1} n_1(r)\,\mathrm{d}r + \int_0^{R_2} n_2(r)\,\mathrm{d}r\right). \tag{22}$$

Again, in the equal radius setup (see appendix B 2 for the general non equal radius result), this quantity is evaluated to be

$$\mathcal{L} = \frac{\pi\hbar}{2}(n_1 + n_2)R^2. \tag{23}$$

For an off-axis vortex at a radius b in the equal radius system, we similarly evaluate the angular momentum,

$$\mathcal{L}(b) = \frac{\pi\hbar}{2}(n_1 + n_2)\left(R^2 - 2b^2 + \frac{b^4}{R^2}\right). \tag{24}$$

For $b \ll R$, this simplifies to

$$\mathcal{L}(b) = \frac{\pi\hbar R^2}{2}(n_1 + n_2)\left(1 - \frac{2b^2}{R^2}\right). \tag{25}$$

These quantities will be helpful when we compute the critical and metastability onset angular velocities in sectionIII C (along the lines of [11]).

C. Theoretical Model in a Rotating Harmonic Trap

Next suppose that we rotate the trap in section III B with an angular velocity Ω. Suppose the state with an-

gular momentum L has energy E_L. This state will be energetically favorable compared to the ground state E_0 if Ω exceeds a critical value Ω_c,

$$\Omega_c = \frac{E_L - E_0}{L} \tag{26}$$

For a single vortex in the Thomas-Fermi regime, we computed $E_L - E_0$ and L in section III B (Eqs. (B5) and (B6)). Using the equal radius assumption, we find that the *critical angular velocity* Ω_c is given by

$$\Omega_c = \frac{2\hbar}{m(n_1+n_2)R^2}\left(\frac{n_1}{2}\sqrt{\frac{n_1 g_{11}}{n_2 g_{22}}} + \frac{n_2}{2}\sqrt{\frac{n_2 g_{22}}{n_1 g_{11}}} + g_{12}\sqrt{\frac{n_1 n_2}{g_{11} g_{22}}} + (n_1+n_2)\log\left(0.539\frac{R}{\xi}\right)\right). \tag{27}$$

To find the *metastability onset angular velocity* Ω_m, we first compute the energy of an off-axis vortex in the equal radius system using the rotating frame. This energy is given by $\tilde{E} = E - \mathbf{\Omega}\cdot\mathbf{L}$. Using results from section III B,

$$\tilde{E}(b) = \epsilon_v \cdot \left(1 - \frac{b^2}{R^2}\right) - \Omega\mathcal{L}\cdot\left(1 - \frac{2b^2}{R^2}\right), \tag{28}$$

where b is the distance of the vortex from the center (and we assume $b \ll R$), and ϵ_v and $\mathcal{L}$ are the quantities in Eqs. (21) and (23). We observe that $\tilde{E}(b)$ has a local minimum at $b = 0$ iff $\Omega \geq \Omega_c/2$, i.e., for $\Omega \geq \Omega_c/2$ we have $\tilde{E}'(b) = 0$ and $\tilde{E}''(b) \geq 0$. So for angular velocities above $\Omega_c/2$, a vortex at the center is locally stable. Therefore, we conclude that the metastability onset angular velocity Ω_m is indeed $\Omega_c/2$.

D. Computational Analysis

In this section we outline the use of the shooting method (see [12] for an introduction) to verify the computational accuracy of the ansatz used in section III A. We first introduce a set of pseudoparameters, listed in Table II.

We would like to solve the following system of ODEs, with boundary conditions $\chi_i(0) = 0$ and $\chi_i(\infty) = 1$,

$$-\frac{1}{x}\frac{d}{dx}\left(x\frac{d\chi_1}{dx}\right) + \frac{\chi_1}{x^2} + a_1\chi_1^3 + a_2\chi_1\chi_2^2 = a_3\chi_1, \tag{29}$$

$$-\frac{1}{x}\frac{d}{dx}\left(x\frac{d\chi_2}{dx}\right) + \frac{\chi_2}{x^2} + b_1\chi_2^3 + b_2\chi_2\chi_1^2 = b_3\chi_2. \tag{30}$$

When changing variables, $u = x/(1+x)$, the boundary conditions transform to $\chi_i(u=0) = 0$ and $\chi_i(u=1) = 1$. Furthermore, we define $y_i = \frac{d\chi_i}{dx}$. The shooting method can then be applied to the system of ODEs obtained by rewriting Eqs. (29) and (30) using these redefinitions (see also appendix B 3). Fig. 6 shows the results using the generic pseudoparameter values in Table II as

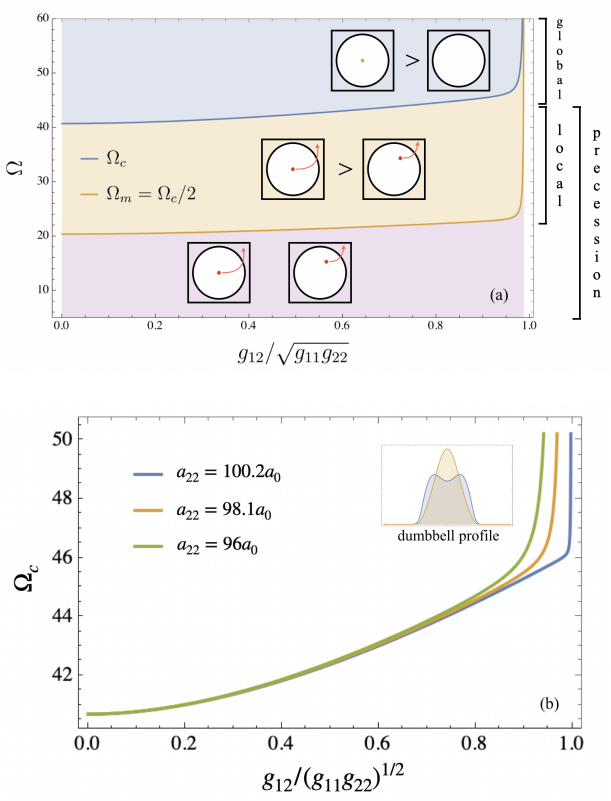

FIG. 5: (a) Phase diagram of a single vortex in a binary condensate system marked with schematics for the various regimes. The vertical axis represents Ω, the angular velocity of the rotating harmonic trap, and the horizontal axis represents the scaled interaction parameter $g_{12}/\sqrt{g_{11}g_{22}}$. Ω_c demarcates the zones of *global stability* (marked "global," blue tier in the figure) and *precession*. For $\Omega > \Omega_c$, an on-center vortex is globally stable, i.e., an on-center vortex state is energetically preferred over the no-vortex state. If $\Omega < \Omega_c$, any vortex formed within the system eventually precesses out of the condensates. The region $\Omega_m < \Omega < \Omega_c$ represents the zone of *local stability* (marked "local", orange tier in the figure). Within this region, an on-center vortex state is energetically preferred over an off-center vortex state, but is not preferred over a no-vortex state. (b) Dependence of the critical angular velocity Ω_c of the binary system on the scaled interaction parameter $g_{12}/\sqrt{g_{11}g_{22}}$ for three different values of a_{22}, the scattering length of the second condensate (or equivalently, the intra-interaction parameter g_{22} of the second condensate), fixing a_{11} at $100.4a_0$. The figure shows a divergence point shifting towards the transition point at $g_{12} = \sqrt{g_{11}g_{22}}$, as the difference between a_{11} and a_{22} (or equivalently between g_{11} and g_{22}) decreases. The inset captioned "dumbbell profile" is a qualitative depiction of the radial profile of the system after the divergence point is reached, in a phase we refer to in section III E as the *dumbbell phase*.

inputs. This numerical solution of the coupled ODEs demonstrates that the simplified ansatz used in section III A is reasonably accurate.

Shooting Method Pseudoparameters		
Parameter	Definition	Test Values
a_1	$\sqrt{(n_1 g_{11})/(n_2 g_{22})}$	1
a_2	$(g_{12}/g_{22}) \cdot (1/a_1)$	0.1
a_3	$a_1 + (g_{12})/(g_{11} a_1)$	1
b_1	$1/a_1$	1
b_2	$(g_{12} a_1)/g_{11}$	0.1
b_3	$1/a_1 + (g_{12} a_1)/g_{22}$	1

TABLE II: Table of pseudoparameters used for the shooting method calculations in section III D. The first column provides the (pseudo)parameter, the second column its definition in terms of quantities introduced in sections II and III A, and the final column provides test values used to plot the results shown in Fig. 6. Particularly, n_j is the j-th condensate's density far from the vortex, g_{jj} is the intra-condensate interaction parameter of the j-th condensate, and g_{ij} (for $i \neq j$) is the inter-condensate interaction parameter.

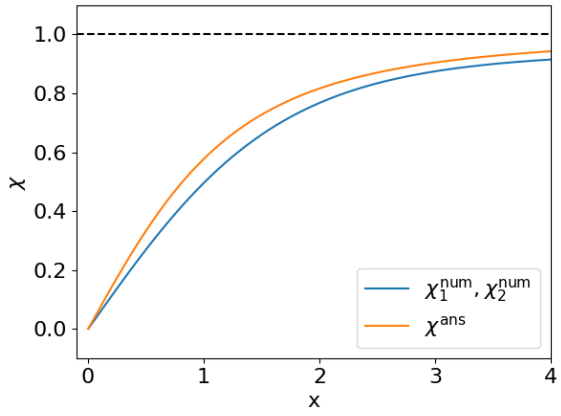

FIG. 6: Numerically obtained (scaled) radial profiles χ_i^{num} of a system of binary condensates in a uniform medium with a singly quantized on-center vortex, compared with the variational ansatz $\chi^{\text{ans}}(x) = x/(2+x^2)^{1/2}$ proposed in section III A. The quantity x on the horizontal axis of the plot is the radial distance ρ scaled by the *aggregate healing length* $\xi = \sqrt{\xi_1 \xi_2}$. The profiles χ_i^{num} were obtained applying the shooting method detailed in section III D over $N = 10000$ steps on the interval $u = 10^{-3}$ to $u = 0.95$, using the values for the pseudoparameters listed in Table I. Here u is the scaled distance $u = x/(1+x)$ used to enforce the boundary conditions at $x = 0$ and $x = \infty$. This figure illustrates the proximity between the numerical solutions and the variational ansatz.

E. Discussion

In this section, we analyze the results from section III C, and specifically the divergences observed in (b) in Fig. 5. The subfigure shows plots of Ω_c against the inter-condensate interaction for narrow and wide separations between g_{11} and g_{22}. The first remarkable aspect of the plot are the stronger-than-polynomial divergences that all occur before the transition point at $g_{12} = \sqrt{g_{11} g_{22}}$. What we see is that as the difference between the intra-condensate interactions (quantified as g_{11}, g_{22}) widens, the divergence point appears earlier as we increase the inter-condensate interactions down and as the difference between the intra-interactions narrows, the divergence point appears later. In the limit that $g_{11} = g_{22}$, this divergence appears to be instantaneous at the transition point, like a pulse.

We propose that this behavior of the divergence point can be physically explained as follows. We first begin with the density profile of the system in the miscible phase in the absence of rotation (see the left side of Fig. 2 for the characteristic 2D profile in this regime). For simplicity, we may further restrict our renditions going forth in this section to the 1D profiles described in [1] (these profiles can be visualized as two concentric inverted parabolas, with slightly different peak heights). As the inter-interaction g_{12} is increased toward the transition point, one sees that the weaker condensate (that is to say, the condensate with smaller Ng_{ii}) holds the center, while the stronger condensate (with larger Ng_{ii}) begins to split into a bimodal state about the central condensate (as in the inset in Fig. 5 (b)). While this is still in the mixing phase (since the centers of both condensates are aligned), the formation of a bimodal state indicates a new subregime that has consistently been observed in the ground states of binary ^{87}Rb-^{87}Rb condensate systems. We term this subregime the *dumbbell phase*.

The physical analogy is this: one can imagine spinning a bowling ball by its center, this is roughly what an on-center vortex must accomplish to be globally stable for lower values of g_{12}. Now as the the ball slowly splits into a dumbbell (whose axle continues to extend), if we were to continue to spin it by the center of the axle, this task certainly takes much more effort (and an increasing amount of effort at that, as the axle extends). This is roughly what an on-center vortex must accomplish to be globally stable once we enter the dumbbell phase, thus requiring an unexpectedly larger value of Ω_c. In more precise terms, there is a divergence in the variance of the condensate distribution (which precisely corresponds to the moment of inertia of the condensate system about an axis passing through the center of the trap) as we enter the dumbbell phase, which results in the corresponding divergences in (b) in Fig. 5.

Before accepting this analogy, one might ask how the entry point to the dumbbell phase varies with wider and narrower gaps between the intra-interactions as in Fig.

5. We see that for 1D systems, as the gap between the intra-interactions g_{11} and g_{22} is narrowed down to near 0, there is virtually no dumbbell phase! (Or better said, the dumbbell phase seems to be instantaneous.) Similarly, as this gap is widened, the dumbbell phase appears earlier as we scale the g_{12} interaction, as one would expect. The remarkable result from this analogy is that we have been able to observe a novel phase in the ^{87}Rb-^{87}Rb condensate system (even in non-rotating contexts), purely informed by the vortex dynamics of the system placed in a rotating trap.

IV. CONCLUSION

In this work, we have discussed the formation and stability of singly quantized vortices in a system of binary BECs. We began in section II with two non-rotating condensates to understand the vortex-free theory. Here we employed a variational analysis on this system and were able to note a phase transition between a *miscible* and an *immiscible* phase as one scales the inter-interaction parameter g_{12}. In section III we began our step-by-step analysis of a binary system of interacting rotating BECs. We began in subsection III A by understanding the theory of a binary BEC system in uniform medium with a singly quantized on-center vortex. Particularly, we derived a form for the asymptotic densities of the condensates, and an approximate form for the vortex energy of the system. In subsection III B, we set our system in a harmonic trap and derive forms for the vortex energy of the system, as well as the total angular momentum of the system. Here, we also provided arguments for the vortex energy and total system angular momentum associated to an off-center vortex at a distance b away from the center. In subsection III C we rotated the trap with an angular velocity Ω and analyzed vortex stability regimes (and corresponding cutoff angular velocities) that are observed for single condensate systems in classical literature (see [2–8] for examples). We checked our work in subsection III A computationally using the shooting method in III D, and the results were remarkably close to the ansatz used in our analysis. Finally, in subsection III E we discussed the presence of a novel *dumbbell phase* for binary BECs (with or without vortices) informed by our analyses of vortex formation and stability in the system. It is curious that this phase had missed most eyes (even in earlier work, see [1]) until we began looking at the vortex stability in the system where it naturally manifests itself.

It remains to concretely understand what quantitative parameters govern the dumbbell phase. As mentioned in subsection III E, returning to mechanical intuition, one way to do this is to numerically obtain the moment of inertia of the system (which in our context, is simply the variance of the condensate distributions), and check for divergences as we tune the interaction parameter g_{12}. At the moment, we do not have a tunable (numerical) form for the condensate wavefunctions in section II, and hence obtaining plot for the moment of inertia of the system is out of our reach as of yet. It is also certainly possible that there is a simple quantitative indicator of bimodality in a distribution that makes the presence of a dumbbell phase apparent, providing an order parameter for this phase.

- ~~Summary of paper, recounting the work in sections II, III A, III B, III C, III D, III E.~~
- ~~Note the significance of being able to discover a new phase of the system by looking at vortex stability~~. Discuss how this phase might be attained in experiment, and ~~quantitative ways to formalize the idea of this subregime.~~
- Remark on how to extend work done in [2–8] to binary systems.
- Remark on extension to multiply quantized vortices, vortex lattices, etc.
- Closing remark on non-trivial behavior due to nonlinear interactions, as observed in [1] and many other articles.

ACKNOWLEDGMENTS

The authors acknowledge the Center for Advanced Research Computing (CARC) at the University of Southern California for providing computing resources that have contributed to the research results reported within this publication. URL: https://carc.usc.edu.

Appendix A: Variational Analysis in Section II

In this appendix, we present key details of the variational analysis within the setup considered in section II, leading to the expressions for σ_x, σ_y, and δ in Eqs. (8), (9), and (10).

Beginning with the evaluated energy functional in Eq. (6), we differentiate with respect to the variational parameters to obtain the ground state conditions for the system,

$$\begin{aligned} &-\frac{\hbar^2}{2m\sigma_{1x}^4}-\frac{Ng_{11}}{4\pi\sigma_{1y}\sigma_{1x}^3}+\frac{1}{2}m\omega_x^2 \\ &=\frac{Ng_{12}(\sigma_{1x}^2+\sigma_{2x}^2-2\delta_x^2)e^{-\frac{\delta_x^2}{\sigma_{1x}^2+\sigma_{2x}^2}-\frac{\delta_y^2}{\sigma_{1y}^2+\sigma_{2y}^2}}}{\pi(\sigma_{1x}^2+\sigma_{2x}^2)^2\sqrt{(\sigma_{1x}^2+\sigma_{2x}^2)(\sigma_{1y}^2+\sigma_{2y}^2)}}, \end{aligned} \tag{A1}$$

$$-\frac{\hbar^2}{2m\sigma_{2x}^4}-\frac{Ng_{22}}{4\pi\sigma_{2y}\sigma_{2x}^3}+\frac{1}{2}m\omega_x^2 = \frac{Ng_{12}(\sigma_{1x}^2+\sigma_{2x}^2-2\delta_x^2)e^{-\frac{\delta_x^2}{\sigma_{1x}^2+\sigma_{2x}^2}-\frac{\delta_y^2}{\sigma_{1y}^2+\sigma_{2y}^2}}}{\pi(\sigma_{1x}^2+\sigma_{2x}^2)^2\sqrt{(\sigma_{1x}^2+\sigma_{2x}^2)(\sigma_{1y}^2+\sigma_{2y}^2)}}, \tag{A2}$$

$$-\frac{\hbar^2}{2m\sigma_{1y}^4}-\frac{Ng_{11}}{4\pi\sigma_{1y}^3\sigma_{1x}}+\frac{1}{2}m\omega_y^2 = \frac{Ng_{12}(\sigma_{1y}^2+\sigma_{2y}^2-2\delta_y^2)e^{-\frac{\delta_x^2}{\sigma_{1x}^2+\sigma_{2x}^2}-\frac{\delta_y^2}{\sigma_{1y}^2+\sigma_{2y}^2}}}{\pi(\sigma_{1y}^2+\sigma_{2y}^2)^2\sqrt{(\sigma_{1x}^2+\sigma_{2x}^2)(\sigma_{1y}^2+\sigma_{2y}^2)}}, \tag{A3}$$

$$-\frac{\hbar^2}{2m\sigma_{2y}^4}-\frac{Ng_{22}}{4\pi\sigma_{2y}^3\sigma_{2x}}+\frac{1}{2}m\omega_y^2 = \frac{Ng_{12}(\sigma_{1y}^2+\sigma_{2y}^2-2\delta_y^2)e^{-\frac{\delta_x^2}{\sigma_{1x}^2+\sigma_{2x}^2}-\frac{\delta_y^2}{\sigma_{1y}^2+\sigma_{2y}^2}}}{\pi(\sigma_{1y}^2+\sigma_{2y}^2)^2\sqrt{(\sigma_{1x}^2+\sigma_{2x}^2)(\sigma_{1y}^2+\sigma_{2y}^2)}}, \tag{A4}$$

$$\delta_x\left(\frac{4Ng_{12}e^{-\frac{\delta_x^2}{\sigma_{1x}^2+\sigma_{2x}^2}-\frac{\delta_y^2}{\sigma_{1y}^2+\sigma_{2y}^2}}}{\pi(\sigma_{1x}^2+\sigma_{2x}^2)\sqrt{(\sigma_{1x}^2+\sigma_{2x}^2)(\sigma_{1y}^2+\sigma_{2y}^2)}}-m\omega_x^2\right)=0, \tag{A5}$$

$$\delta_y\left(\frac{4Ng_{12}e^{-\frac{\delta_x^2}{\sigma_{1x}^2+\sigma_{2x}^2}-\frac{\delta_y^2}{\sigma_{1y}^2+\sigma_{2y}^2}}}{\pi(\sigma_{1y}^2+\sigma_{2y}^2)\sqrt{(\sigma_{1x}^2+\sigma_{2x}^2)(\sigma_{1y}^2+\sigma_{2y}^2)}}-m\omega_y^2\right)=0. \tag{A6}$$

Applying the balance relation Eq. (7) in section II to the ground state conditions above, we obtain the simplifications

$$\sigma_x^4=\frac{Ng_{12}\omega_y e^{-\frac{\delta_x^2}{2\sigma_x^2}-\frac{\delta_y^2}{2\sigma_y^2}}}{\pi m\omega_x^3}, \tag{A7}$$

$$\sigma_y^4=\frac{Ng_{12}\omega_x e^{-\frac{\delta_x^2}{2\sigma_x^2}-\frac{\delta_y^2}{2\sigma_y^2}}}{\pi m\omega_y^3}, \tag{A8}$$

$$-\frac{\hbar^2}{2m\sigma_x^4}-\frac{N\omega_y g}{4\pi\sigma_x^4\omega_x}+\frac{1}{2}m\omega_x^2=\frac{Ng_{12}\omega_y(\sigma_x^2-\delta_x^2)e^{-\frac{\delta_x^2}{2\sigma_x^2}-\frac{\delta_y^2}{2\sigma_y^2}}}{4\pi\sigma_x^6\omega_x}, \tag{A9}$$

$$-\frac{\hbar^2}{2m\sigma_y^4}-\frac{N\omega_x g}{4\pi\sigma_y^4\omega_y}+\frac{1}{2}m\omega_x^2=\frac{Ng_{12}\omega_x(\sigma_y^2-\delta_y^2)e^{-\frac{\delta_x^2}{2\sigma_x^2}-\frac{\delta_y^2}{2\sigma_y^2}}}{4\pi\sigma_y^6\omega_y}. \tag{A10}$$

To simplify the situation further, as mentioned in section II, we drop the kinetic terms from Eqs. (A9) and (A10) (this is consistent with the large N limit). We also restrict ourselves to separation only along the x-direction, so that $\delta_y=0$ and $\delta:=\delta_x\geq 0$. This resolves the ground state conditions further to

$$\sigma_x^4=\frac{Ng_{12}\omega_y e^{-\frac{\delta^2}{2\sigma_x^2}}}{\pi m\omega_x^2}, \tag{A11}$$

$$\sigma_y^4=\frac{Ng_{12}\omega_x e^{-\frac{\delta^2}{2\sigma_x^2}}}{\pi m\omega_y^2}, \tag{A12}$$

$$-\frac{N\omega_y g}{4\pi\sigma_x^4\omega_x}+\frac{1}{2}m\omega_x^2=\frac{Ng_{12}\omega_y(\sigma_x^2-\delta^2)e^{-\frac{\delta^2}{2\sigma_x^2}}}{4\pi\sigma_x^6\omega_x}, \tag{A13}$$

$$-\frac{N\omega_x g}{4\pi\sigma_y^4\omega_y}+\frac{1}{2}m\omega_y^2=\frac{Ng_{12}\omega_x(\sigma_y^2)e^{-\frac{\delta^2}{2\sigma_x^2}}}{4\pi\sigma_y^6\omega_y}. \tag{A14}$$

For notational convenience, we also set $\mathcal{G}:=e^{-\frac{\delta^2}{2\sigma_x^2}}$. We now focus on Eqs. (A11) and (A13). The condition Eq. (A13) simplifies to

$$\sigma_x^4=\frac{N\omega_y}{2m\pi\omega_x^3}\left(g+\frac{g_{12}(\sigma_x^2-\delta^2)\mathcal{G}}{\sigma_x^2}\right). \tag{A15}$$

Using Eq. (A11), we obtain the expression

$$g/g_{12}=\left(1+\frac{\delta^2}{\sigma_x^2}\right)\mathcal{G}\equiv\left(1+\frac{\delta^2}{\sigma_x^2}\right)e^{-\frac{\delta^2}{2\sigma_x^2}}. \tag{A16}$$

Finally, Eq. (A16) may be Taylor expanded for small δ, and using Eqs. (A11) and (A12) the low-order approximations yield approximations for δ, σ_x, and σ_y.

$$\sigma_x^4=\frac{N\omega_y}{m\pi\omega_x^3}\frac{g+g_{12}}{2}, \tag{A17}$$

$$\sigma_y^4=\frac{N\omega_x}{m\pi\omega_y^3}\frac{g+g_{12}}{2}, \tag{A18}$$

$$\delta=\left(\frac{2N\omega_y}{m\pi\omega_x^3}(g+g_{12})\right)^{1/4}\sqrt{\log_e\left(\frac{g_{12}}{g}\right)}. \tag{A19}$$

Appendix B: Details of Rotating Condensates in Section III

This appendix is a supplement to section III, presenting key details omitted from its subsections for presentation purposes.

1. Vortex Core Sizes

In this subsection, we show that the core size of the vortex considered in section III B (determined by the healing lengths of the condensates) is much smaller than the radii of the condensates (restricting ourselves to the Thomas-Fermi regime of the system). Recall first the relation

$$\frac{\hbar^2}{2m\xi_{0,j}^2} = n_j(0)g_{jj}, \tag{B1}$$

where $\xi_{0,j}$ is the healing length of the j-th condensate ($j = 1, 2$) at the center, and $n_j(0)$ is the density of the j-th condensate at the center in the absence of rotation. As in section III B, we call these quantities ξ_j and n_j, provided there is no concern of ambiguity. The chemical potential of the j-th condensate (μ_j) is related to the trap frequency $\omega_\perp$, and the radius of the j-th condensate (R_j) by the relation

$$\mu_j = \frac{1}{2}m\omega_\perp R_j^2. \tag{B2}$$

From section III A, we also know

$$n_j g_{jj} = \frac{\mu_j - \frac{g_{12}}{g_{ii}}\mu_i}{1 - \frac{g_{12}^2}{g_{11}g_{22}}}, \tag{B3}$$

where $i \neq j$ and $i, j \in \{1, 2\}$. This leads to the relation

$$\frac{\xi_j}{R_j} = \frac{\hbar\omega_\perp}{2\mu_j}\sqrt{\frac{1 - \frac{g_{12}^2}{g_{11}g_{22}}}{1 - \frac{g_{12}}{g_{ii}}\frac{R_i^2}{R_j^2}}}. \tag{B4}$$

In the Thomas-Fermi regime, the right hand side of Eq. (B4) is small (since the chemical potential μ_j is much larger than the trap energy $\hbar\omega_\perp$), so we conclude that $\xi_j \ll R_j$ in this setup, as desired.

2. Non-Equal Radius Results

In this subsection, we present results from the analysis in section III B and section III C for non equal radius condensates, that is, condensates such that R_1 and R_2 are allowed to be distinct.

By evaluating the integrals in Eq. (20) for a generic pair (R_1, R_2), we obtain the vortex energy per unit length,

$$\begin{aligned}\epsilon_v = {} & \frac{\pi\hbar^2}{m}n_1\left(\frac{1}{2}\sqrt{\frac{n_1 g_{11}}{n_2 g_{22}}} + \log\left(0.888\frac{R_1}{\xi}\right)\right. \\ & \left. - \frac{(g_{12} - g_{22})R_1^2}{2(g_{12}R_2^2 - g_{22}R_1^2)}\right) \\ & + \frac{\pi\hbar^2}{m}n_2\left(\frac{1}{2}\sqrt{\frac{n_2 g_{22}}{n_1 g_{11}}} + \log\left(0.888\frac{R_2}{\xi}\right)\right. \\ & \left. - \frac{(g_{12} - g_{11})R_2^2}{2(g_{12}R_1^2 - g_{11}R_2^2)}\right) \\ & + \frac{\pi\hbar^2}{m}g_{12}\sqrt{\frac{n_1 n_2}{g_{11}g_{22}}}.\end{aligned} \tag{B5}$$

Similarly, by evaluating in the integrals in Eq. (22) for a generic pair (R_1, R_2), obtain the angular momentum of the system to be

$$\begin{aligned}\mathcal{L} = \frac{\pi\hbar}{2}\left(2n_1R_1^2 + n_1\frac{g_{12} - g_{22}}{g_{22}R_1^2 - g_{12}R_2^2}R_1^4 + 2n_2R_2^2\right. \\ \left. + n_2\frac{g_{12} - g_{11}}{g_{11}R_2^2 - g_{12}R_1^2}R_2^4\right).\end{aligned} \tag{B6}$$

As in section III C, this gives us enough information to compute the critical angular velocity Ω_c when $R_1 \neq R_2$. The result of this, of course, is just the quotient of Eq. (B5) by Eq. (B6).

3. Shooting Method

In this subsection, we present the system of ODEs obtained by rewriting the GPEs in Eqs. (29) and (30) after the change of variables enforcing the boundary conditions (see section III D for these redefinitions). The system of ODEs thus obtained is

$$\begin{aligned}\frac{d\chi_i}{du} &= \frac{y_i}{(1-u)^2} \\ \frac{dy_1}{du} &= \frac{a_1\chi_1^3}{(1-u)^2} + \frac{a_2}{(1-u)^2}\chi_1\chi_2^2 - \frac{y_1}{u(1-u)} \\ &\quad + \frac{\chi_1}{u^2} - \frac{a_3\chi_1}{(1-u)^2} \\ \frac{dy_2}{du} &= \frac{b_1\chi_2^3}{(1-u)^2} + \frac{b_2}{(1-u)^2}\chi_2\chi_1^2 - \frac{y_2}{u(1-u)} \\ &\quad + \frac{\chi_2}{u^2} - \frac{b_3\chi_2}{(1-u)^2}\end{aligned} \tag{B7}$$

where $i \in \{1, 2\}$. The results from the analysis presented in section III D are now obtained by applying the shooting method to Eq. (B7).

[1] A. Wirthwein, S. Haas, and S. wey Chiow, Collision Dynamics of Bose-Einstein Condensates, (2022), arXiv:2203.11104 [cond-mat.quant-gas].

[2] A. L. Fetter, Rotating trapped Bose-Einstein condensates, Laser Physics **18**, 1–11 (2008).

[3] W. Bao, Q. Du, and Y. Zhang, Dynamics of Rotating Bose–Einstein Condensates and its Efficient and Accurate Numerical Computation, SIAM Journal on Applied Mathematics **66**, 758 (2006), https://doi.org/10.1137/050629392.

[4] B. P. Anderson, P. C. Haljan, C. E. Wieman, and E. A. Cornell, Vortex Precession in Bose-Einstein Condensates: Observations with Filled and Empty Cores, Phys. Rev. Lett. **85**, 2857 (2000).

[5] I. Coddington, P. C. Haljan, P. Engels, V. Schweikhard, S. Tung, and E. A. Cornell, Experimental studies of equilibrium vortex properties in a Bose-condensed gas, Physical Review A **70**, 10.1103/physreva.70.063607 (2004).

[6] A. L. Fetter and A. A. Svidzinsky, Vortices in a trapped dilute Bose-Einstein condensate, Journal of Physics: Condensed Matter **13**, R135–R194 (2001).

[7] G. M. Kavoulakis, B. Mottelson, and C. J. Pethick, Weakly interacting Bose-Einstein condensates under rotation, Physical Review A **62**, 10.1103/physreva.62.063605 (2000).

[8] K. W. Madison, F. Chevy, W. Wohlleben, and J. Dalibard, Vortex Formation in a Stirred Bose-Einstein Condensate, Physical Review Letters **84**, 806–809 (2000).

[9] M. Egorov, B. Opanchuk, P. Drummond, B. V. Hall, P. Hannaford, and A. I. Sidorov, Measurement of s-wave scattering lengths in a two-component Bose-Einstein condensate, Physical Review A **87**, 10.1103/physreva.87.053614 (2013).

[10] L. Pitaevskii and S. Stringari, *Bose-Einstein Condensation*, International Series of Monographs on Physics (Clarendon Press, 2003).

[11] C. Pethick and H. Smith, *Bose-Einstein Condensation in Dilute Gases* (Cambridge University Press, 2002).

[12] T. Pang, *An Introduction to Computational Physics* (Cambridge University Press, 2006).

[13] F. Dalfovo, S. Giorgini, L. P. Pitaevskii, and S. Stringari, Theory of bose-einstein condensation in trapped gases, Reviews of Modern Physics **71**, 463–512 (1999).

[14] A. N. da Silva, R. K. Kumar, A. S. Bradley, and L. Tomio, Vortex generation in stirred binary Bose-Einstein condensates, Phys. Rev. A **107**, 033314 (2023).

[15] M. N. Tengstrand, P. Stürmer, E. O. Karabulut, and S. M. Reimann, Rotating binary bose-einstein condensates and vortex clusters in quantum droplets, Phys. Rev. Lett. **123**, 160405 (2019).

[16] R. Doran, A. W. Baggaley, and N. G. Parker, Vortex solutions in a binary immiscible bose-einstein condensate, Phys. Rev. A **109**, 023318 (2024).

[17] K. Kasamatsu, M. Tsubota, and M. Ueda, Vortex phase diagram in rotating two-component bose-einstein condensates, Phys. Rev. Lett. **91**, 150406 (2003).